Influence of the absorber doping for *p*-type polycrystalline silicon thin-film solar cells on glass prepared by electron beam evaporation and solid-phase crystallization

Zi Ouyang,[a] Oliver Kunz,[b] Alistair B. Sproul, and Sergey Varlamov
ARC Photovoltaics Centre of Excellence, University of New South Wales, Sydney, NSW 2052, Australia

(Received 4 September 2010; accepted 12 January 2011; published online 15 March 2011)

A systematic investigation of the influence of the absorber doping on the performance of planar, *p*-type, evaporated, solid-phase crystallized polycrystalline silicon thin-film solar cells on glass is presented. It is found that the optimum Suns-V_{oc} parameters (open-circuit voltage and pseudo fill factor) are achieved at intermediate absorber doping of $N_{abs}\sim 1–2\times 10^{17}$ cm^{-3}, while high short-circuit currents are achieved at the lowest absorber doping of $N_{abs}\leq 6\times 10^{15}$ cm^{-3}. Since the short-circuit current is the dominating factor to achieve high conversion efficiencies for evaporated polycrystalline silicon cells, the maximum pseudo efficiencies are achieved at very low absorber doping. The Suns-V_{oc} characteristics of lightly doped cells can be adequately described by a modified two-diode model with $n_1=1$ and $n_2\approx 1.5$, which is in contrast to the value of 2 for n_2 commonly quoted in the literature. PC1D modeling demonstrates that such a low ideality factor for space charge region recombination can be modeled by a single trap energy level located at ~0.18 eV away from midgap. Although the achievable short-circuit current densities and the conversion efficiencies can be higher for textured cells, planar cells are chosen intentionally to allow accurate modeling and extraction of relevant material parameters, such as minority carrier diffusion length.
© *2011 American Institute of Physics*. [doi:10.1063/1.3553886]

I. INTRODUCTION

Thin-film polycrystalline silicon (poly-Si) on glass is a promising emerging thin-film photovoltaic technology. It has the advantages of crystalline Si technology, low material usage, large-area monolithic construction typical for the thin-film approach, and avoids the use of additional cell encapsulation by taking advantage of the transparent glass superstrates.[1] The conventional approach for deposition of the precursor *a*-Si diodes is plasma enhanced chemical vapor deposition (PECVD).[2–4] However, PECVD has relatively low deposition rates[2,3] (typically <60 nm/min), which makes it expensive for mass production of poly-Si thin films for thicknesses exceeding 1 μm. There are two general approaches used to overcome this problem. One is to increase the deposition rate by increasing the rf power and frequency; most recently, a 250 nm/min deposition rate without performance degradation was reported.[5] Another approach is to replace PECVD with faster deposition processes such as electron beam (e-beam) evaporation, where a deposition rate of 600 nm/min has been demonstrated for Si photovoltaic devices[6] and rates well above 1 μm/min are believed to be possible. Recently, a 5.2% efficiency was achieved for planar evaporated solid-phase crystallized (SPC) poly-Si thin-film solar cells with interdigitated line contact metallization;[7] a 6.7% efficiency was realized with a more advanced point contact metallization;[6] and with the addition of Si surface texturing, this has resulted in a 7.4% efficiency.[6] Higher efficiencies require the implementation of more effective light trapping schemes that are compatible with the deposition process to improve the photocurrent.[8] At the same time, achieving high open-circuit voltages requires a better understanding of the evaporated poly-Si material properties and how they are affected by the deposition conditions and the film structure.[9] In this paper, the aim is to investigate an important aspect of evaporated poly-Si thin-film cells: the influence of the absorber doping N_{abs} on the device performance parameters, namely the open-circuit voltage V_{oc}, pseudo fill factor pFF, short-circuit current density J_{sc}, and pseudo efficiency pEff.

For *p*-type monocrystalline Si wafer cells, it has been shown that the maximum J_{sc} occurs at an absorber doping of $\sim 10^{15}$ cm^{-3} or lower, while the maximum V_{oc} occurs at $\sim 10^{17}$ cm^{-3}. The highest efficiencies are obtained at absorber doping levels of about 10^{15} cm^{-3}.[10] Similar trends for J_{sc} and efficiency η have been found on *p*-type block cast multicrystalline silicon wafer solar cells.[11] The most similar cell type to those investigated in this work are e-beam evaporated solar cells making use of ion-assisted deposition on seed layers prepared by aluminum-induced crystallization. Owing to the *p*-type nature of the seed layer, these poly-Si thin-film solar cells have *n*-type absorber layers. The maximum J_{sc} and V_{oc} occurred at $\sim 10^{17}$ cm^{-3} doping, and the minimum J_{sc} and V_{oc} at $\sim 10^{16}$ cm^{-3}.[12] The aforementioned investigations showed that varying the absorber doping from 10^{15} to 10^{18} cm^{-3} results in large efficiency differences that can be as high as 80% for wafer cells and even 400% for

[a]Now with Victoria-Suntech Advanced Solar Facility, Swinburne University of Technology, Melbourne VIC 3122, Australia. Electronic mail: ouyangzi@gmail.com.
[b]Present address: CSG Solar Pty Ltd, 82 Bay Street, Botany NSW 2019, Australia.

 © 2011 American Institute of Physics

Downloaded 26 Mar 2012 to 136.186.72.84. Redistribution subject to AIP license or copyright; see http://jap.aip.org/about/rights_and_permissions

thin-film cells. This reveals the importance of the investigation of the impact of absorber doping on the device performance for *p*-type evaporated SPC poly-Si solar cells on glass, which has not been reported previously.

A number of different solar cell parameters were investigated during this study to examine the impact of absorber doping. In comparison to the fill factor (FF) and η from light *I–V* measurements, the parameters' pFF extracted from Suns-V_{oc} and pEff extracted from Suns-V_{oc} and external quantum efficiency (EQE) measurements are independent of the metallization scheme in use and therefore preferable for investigating the properties of the evaporated poly-Si thin-film material. Nonetheless, FF and Eff are briefly presented for completeness. Other parameters such as the thickness of the absorber t_{abs} and the effective diffusion length of minority carriers in the absorber L_{eff} are determined by modeling EQE data utilizing the solar cell modeling program PC1D.[13] Additionally, the ideality factors n_1 and n_2, which are important two-diode model parameters, were extracted by fitting the experimental Suns-V_{oc} data to the two-diode model. This allows one to draw important conclusions regarding the dominant recombination mechanisms for the studied cells.

II. SAMPLE PREPARATION

Evaporated poly-Si solar cells with different absorber doping were prepared for this study. The amorphous Si precursor thin films were deposited by e-beam evaporation ($\sim 10^{-7}$ Torr deposition pressure) on *planar* borosilicate glass substrates coated with a silicon nitride (SiN_x) barrier and AR coating. The film structure consists of a thin phosphorus-doped emitter (deposited at ~100 nm/min) followed by boron-doped absorber (at ~300 nm/min), and back surface field [(BSF), at ~40 nm/min]. Doping of the layers was achieved during the Si film deposition process using boron and phosphorus effusion cells. The absorber doping was controlled by the temperature of the boron effusion cell. After deposition the films underwent SPC, rapid thermal annealing (RTA), and hydrogen plasma passivation (hydrogenation). The design parameters of the cells are shown in Table I. With the exception of the absorber doping, all films are nominally identical. For comprehensive characterization, the poly-Si films were then patterned into cells with an area of 2 cm^2 using interdigitated Al line contacts on both the emitter and the BSF layers. After metallization, a simple back surface reflector (BSR) consisting of white paint was applied to the rear cell surface to improve the light trapping. The cell structure is illustrated in Fig. 1. More details on the metallization scheme used in this work are given in Ref. 14. Textured cells were not used for the study as accurate optical and electrical modeling of textured cells is far more difficult and relevant material parameters cannot be as readily extracted as is the case for planar samples.

TABLE I. Design parameters of the evaporated poly-Si cells. The absorber doping is variable.

Parameter	Details
Glass	3.3 mm planar borosilicate glass
AR coating	~70 nm SiN, n~1.9 at 632 nm
Emitter	~50 nm,[a] n^+ doping, 10^{20} cm^{-3}
Absorber	~2.1 μm,[a] p^- doping
BSF	~120 nm, p^- doping, 10^{19} cm^{-3}
SPC	24 h at 600 °C
RTA	4 min at ~900 °C
Hydrogenation	20 min at ~650 °C, remote plasma
BSR	Air or white paint

[a]Real thicknesses are affected by the extensive thermal dopant diffusion, which is discussed in Sec. IV A.

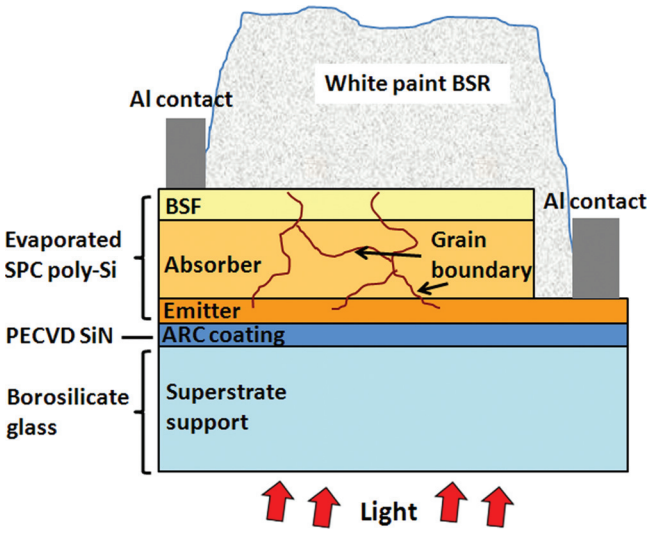

FIG. 1. (Color online) Cross-sectional schematic of an evaporated poly-Si cell in superstrate configuration, i.e., illuminated through the supporting glass. Schematic is not to scale.

III. CHARACTERIZATION AND SIMULATION METHODS

A. Determination of absorber doping N_{abs}

Impedance analysis was used to determine the absorber doping N_{abs} of all cells after metallization. This method enables the accurate determination of the depletion region capacitance even in the presence of parasitic shunt and series resistances, which arise from the metallization. The *active* dopant concentration in the absorber layer was then obtained utilizing the standard *C–V* relationship:

$$\frac{1}{C^2} = \frac{2(V_{bi} - V_a)}{q\varepsilon_0\varepsilon_r A^2 N_{abs}}, \quad (1)$$

where q is the electronic charge, ε_0 the permittivity in vacuum condition, ε_r the relative permittivity of the semiconductor, C the capacitance, A the area, V_{bi} the built-in potential of the junction, V_a the applied voltage at the junction, and N_{abs} the absorber doping. More details on the method used in this work are given in Ref. 15.

B. Determination of V_{oc}, pFF, and ideality factors

Suns-V_{oc} measurements were performed to determine V_{oc}, pFF, and ideality factors of the cells prior to metallization. The Suns-V_{oc} technique was first introduced by Sinton and Cuevas,[16] and since then has been widely applied to

Downloaded 26 Mar 2012 to 136.186.72.84. Redistribution subject to AIP license or copyright; see http://jap.aip.org/about/rights_and_permissions

solar cell characterization.[9,17,18] The quasisteady-state V_{oc} of the sample cell is plotted against varying illumination intensity (in Suns) from a decaying flash lamp pulse (decay constant ~2 ms). A great advantage of this method is that it can be used to measure solar cells at various stages of metallization, and even be applied to nonmetallized cells. It thereby allows the investigation of inherent material properties, which can easily be obscured by metallization-induced factors such as series resistance R_s and shunt resistance R_{sh}. Assuming J_{sc} is proportional to the illumination intensity, Suns-V_{oc} curves can be converted into pseudolight *J-V* curves, i.e., light *J–V* curves in the absence of series resistance effects.[19,20]

The V_{oc} at 1 Sun can be directly measured by the Suns-V_{oc} setup, where 1 Sun illumination is determined by a reference cell. The pFF is a useful performance parameter that represents the maximum fill factor that a cell can reach in the case where R_s=0. It is determined by the following relation:

$$\mathrm{pFF} = \frac{V_{oc}(\mathrm{MPP})J_{norm}(\mathrm{MPP})}{V_{oc}(1\ \mathrm{Sun})}, \tag{2}$$

where V_{oc} (MPP) and J_{norm} (MPP) are the open-circuit voltage and the normalized current density at the maximum power point (MPP) of the pseudolight *I-V* curve, respectively.[16] Note that both V_{oc} and pFF are directly deduced from measurement results without the use of a curve fitting procedure.

To get a better understanding of the fundamental recombination mechanism in these films, we applied two-diode model fits to the Suns-V_{oc} data. A good review of the two-diode model[21] and the specific application to Si thin-film solar cells[22] can be found elsewhere. In the equivalent circuit of this model, two diodes (D_1 and D_2), as well as a shunt resistance, are in parallel with the ideal current source. Conventionally, D_1 models recombination in the quasineutral regions and the surfaces of a diode, and D_2 models recombination in the diode's space charge regions (depletion regions) such as the *p–n* junction and extended defects (e.g., grain boundaries and dislocations). The exponential factors of the two diodes can be described by the so-called ideality factors, n_1 and n_2. As the ideality factors are indicative of the type of recombination, they are useful parameters for the identification of the recombination mechanisms of a solar cell at different injection levels.

The local ideality factor m is another useful parameter. When applied to Suns-V_{oc} data, it is defined by

$$m = \frac{q}{kT}\left(\frac{\Delta V_{oc}}{\Delta \ln(J_{norm})}\right). \tag{3}$$

Typically the *I–V* curve is converted into an *m–V* curve for the observation of subtle details. More details of local ideality factor can be found in Ref. 23. In this work, the *m–V* data measured via Suns-V_{oc} and the data fitted via PC1D and the two-diode model are compared to investigate the relationship between recombination and the absorber doping.

C. Determination of EQE, J_{sc}, and pseudo efficiency

EQE measurements were used to determine the photocurrent of the cells after metallization. The EQE is the ratio of collected (photogenerated) carriers to incident photons as a function of the wavelength under short-circuit conditions.[21] The 1 Sun J_{sc} can be calculated from the EQE data as

$$J_{sc}(\mathrm{EQE}) = q\int \mathrm{EQE}(\lambda)S(\lambda)d(\lambda), \tag{4}$$

where q is the electron charge and $S(\lambda)$ is the standard spectral photon density of sunlight at the earth's surface (air mass 1.5). This approach avoids the use of a solar simulator to measure J_{sc}, and hence avoids the problems associated with spectral mismatch.

The pEff is used in this work as a means of evaluating the cell performance that is unaffected by series resistance effects introduced by the metallization. It is determined from

$$\mathrm{pEff} = J_{sc}(\mathrm{EQE})V_{oc}\mathrm{pFF}. \tag{5}$$

D. Determination of absorber thickness and effective diffusion length

PC1D is a simulation program that solves the fully coupled nonlinear equations for the quasi-one-dimensional transport of electrons and holes in crystalline semiconductor devices, with particular emphasis on photovoltaic devices.[13] It is used to determine the effective diffusion length of minority carriers in the absorber L_{eff} by fitting modeled EQE and reflectance data with experimental data obtained via spectrophotometer measurements. PC1D is also used to determine the trap energies in the depletion region by fitting modeled *m–V* data with data obtained via Suns-V_{oc} measurements.

Lastly, light *I–V* measurements were performed on cells after metallization for completeness purposes.

IV. RESULTS AND DISCUSSION

A. Cell performance versus absorber doping

Twenty-one e-beam poly-Si thin-film solar cells with a wide range of absorber doping ($\sim 2\times10^{15}$ cm^{-3}<N_{abs}<$\sim 8\times10^{17}$ cm^{-3}) were prepared and characterized. Figure 2 shows the important cell performance parameters V_{oc}, pFF, J_{sc}(EQE), and pEff as a function of N_{abs}. The J_{sc}(EQE) was calculated from EQE measurements, which should be distinguished from J_{sc} obtained from light *I–V* measurements. The J_{sc}(EQE) and pEff were determined under two different light-trapping schemes: air and a white paint BSR. The data show a very similar trend for both V_{oc} and pFF, i.e., the values first increase and then, from $N_{abs}\sim 2\times10^{17}$ cm^{-3} on, decrease sharply. The peak V_{oc} of 448 mV and peak pFF of 75.8% were obtained at $N_{abs}=10^{17}$ cm^{-3}. The shape of the trend, as well as the location of the peaks, is very similar to typical wafer-based monocrystalline Si solar cells.[10] However, the highest V_{oc} for the tested evaporated SPC poly-Si thin-film cells is ~150 mV and ~250 mV lower than typical values for commercial and high-efficient lab-type wafer-based Si solar cells, respectively.[21] This indicates a clear need for a reduction in recombination in order to achieve higher open-circuit voltages.

Downloaded 26 Mar 2012 to 136.186.72.84. Redistribution subject to AIP license or copyright; see http://jap.aip.org/about/rights_and_permissions

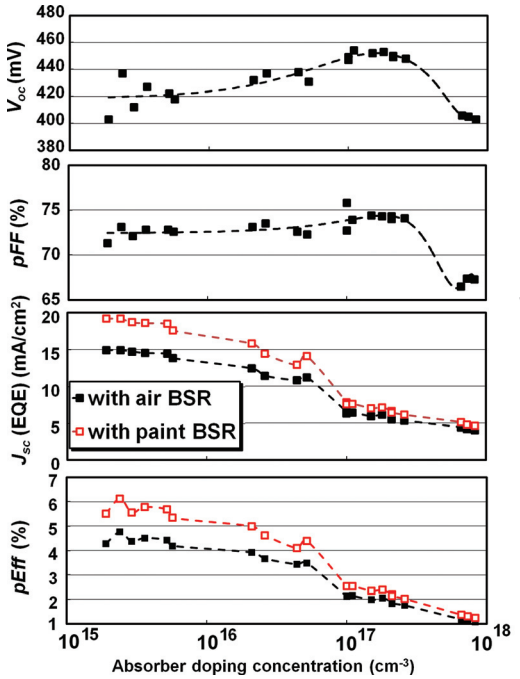

FIG. 2. (Color online) Measured values for V_{oc}, pFF, J_{sc}(EQE), and pEff as a function of the absorber doping. J_{sc} is calculated from EQE results. J_{sc}(EQE) and pEff were obtained under two different backsurface reflector schemes: air (black closed squares) and white paint (red open squares).

Figure 3 compares the EQE curves of the cells that are representative for the samples investigated. The slight EQE difference for wavelengths shorter than 350 nm is due to minor variations in the SiN_x AR coating properties (thickness and stoichiometry). For wavelengths longer than 400 nm the EQE increases with decreasing N_{abs}. With decreasing absorber doping the peak EQE also shifts toward longer wavelengths. As all investigated cells use the same light-trapping scheme, the EQE variation at wavelengths longer than 400 nm has to be related to the properties of the Si material itself. It has been well documented that the effective diffusion length for minority carriers in the absorber L_{eff} and the thickness of the absorber t_{abs} are two major parameters to determine the quantum efficiency of solar cells.[10,21,24] They affect the amount of the light being absorbed in the film and the collection probability of the light-generated carriers, respectively. Most important, L_{eff} needs to be larger than t_{abs} to guaranty that essentially all light-generated carriers are collected by the junction before recombining in the quasi-neutral bulk.

PC1D modeling was carried out to determine L_{eff} and t_{abs}. The cells were modeled without the white paint BSR (i.e.,with air as BSR) since any light trapping scheme introduces uncertainties with respect to carrier generation and thus unnecessarily large errors in the determined material properties. Modeled EQE and optical data were compared with the experimental data to determine the model parameters. A close match was achieved between the experimental and modeled data for all cells. Figure 4 shows the modeled and measured results on a cell with an absorber doping of 2.4×10^{15} cm^{-3}. In spite of the good fit over most of the regions, some minor deviations exist. The deviation of the EQE curves at wavelengths shorter than 400 nm is due to the limitation of PC1D in that it assumes a single value for the refractive index and zero absorption for the SiN_x coating. This then leads to modeled reflectance curves that differ from the experimental data at short wavelengths. Also the measured reflectance results are slightly lower than the modeled ones in the long wavelength regime and no interference fringes are seen in the modeled reflectance curves. This is due to the fact that PC1D only models the noncoherent optical properties and does not include thin-film interference effects. These deviations are considered to have little impact on the modeling quality of L_{eff} and t_{abs}, as both quantities are mainly determined from the data between 400 and 800 nm wavelengths where the absorber plays the dominant role.

To achieve convincing fitting results the following parameters were set as constants: BSF thickness 100 nm, BSF doping 4×10^{19} cm^{-3}, BSF diffusion length 117 nm, refractive indices n_{air}=1 and n_{glass}=1.48. n_{SiN} was included as a fitting parameter with values varying from 1.9 to 2. The rear surface recombination velocity was found to have a negligible effect on all modeling results, indicating that surface

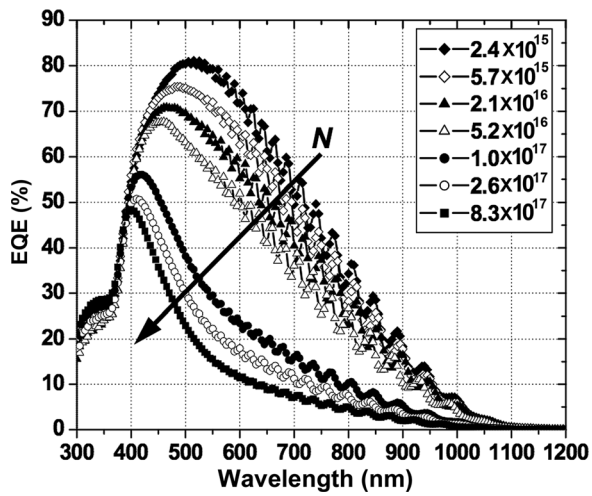

FIG. 3. Measured external quantum efficiency of seven representative cells with different absorber doping. All cells feature a white paint BSR.

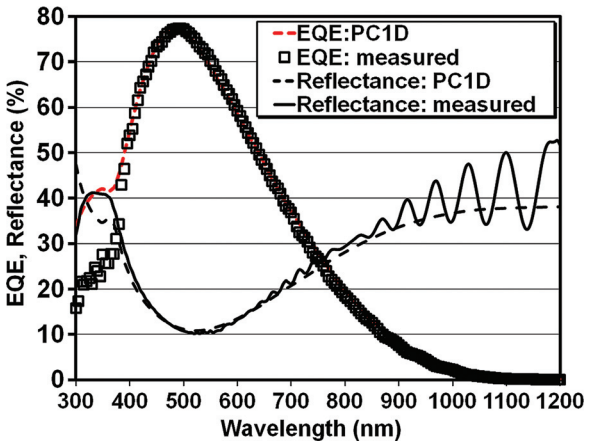

FIG. 4. (Color online) Measured EQE (open black squares), PC1D modeled EQE (red dashed concave line), measured reflectance (black solid line) and PC1D modeled reflectance (black dashed convex line) of a cell with absorber doping of 2.4×1015 cm^{-3} and with air BSR.

Downloaded 26 Mar 2012 to 136.186.72.84. Redistribution subject to AIP license or copyright; see http://jap.aip.org/about/rights_and_permissions

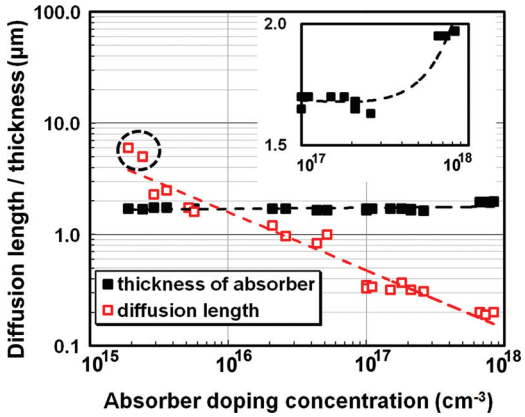

FIG. 5. (Color online) PC1D modeled effective diffusion length (red open squares) and absorber thickness (black closed squares) as a function of the absorber doping. The inset highlights the thickness increase of the absorber at high absorber doping levels.

passivation is not important for the performance of the investigated evaporated Si thin-film cells.[8] The parameters L_{eff} and t_{abs} were adjusted until the experimental data and the model curves were in satisfactory agreement.

It was found that both L_{eff} and t_{abs} are primarily dependent on the absorber doping N_{abs}. As shown in Fig. 5, the L_{eff} values are approximately proportional to the inverse square root of N_{abs}. This result is consistent with the recent findings that the lifetimes in the poly-Si cells vary inversely with the absorber doping.[25] Despite the fact that the deposited thicknesses of the absorber layers were close to identical for all the investigated cells, t_{abs} are still variable. This is due to the fact that the RTA process during cell preparation results in extensive thermal diffusion of phosphorus from the emitter to the absorber.[26] This changes the actual junction location and thereby the absorber thickness. In this study, the change of the actual junction location depends on the absorber doping. For a given phosphorus diffusion profile, the lower the absorber boron doping, the longer the distance over which the change of polarity takes place, and thus, the thinner the absorber becomes. On the contrary, for the higher absorber boron doping less polarity change occurs and the absorber thickness does not change much. This effect can be seen in the inset of Fig. 5 for very heavily doped absorbers, where t_{abs} increases as N_{abs} increases. It is also worth noting that in the case where the diffusion length is more than double the absorber thickness (see the black circle of Fig. 5) the modeling of this parameter becomes less reliable as the collection efficiency is close to unity in the entire absorber region. Therefore in the circle of Fig. 5 high L_{eff} values are to be treated with some care.

As previously discussed, for effective collection of photogenerated carriers L_{eff} should be greater than t_{abs}. According to Fig. 5, this condition is met where N_{abs} falls below $\sim 6 \times 10^{15}$ cm^{-3}, corresponding to the highest quantum efficiencies shown in Fig. 3. One may rely on the relationship shown in Fig. 5 as a guide to determine the combination of cell thickness and absorber doping that will ensure high carrier collection efficiencies.

Measured light *I–V* parameters of four selected metallized cells are shown in Table II. It is evident that the

TABLE II. Light *I–V* characteristics of four selected cells with different absorber doping.

Doping (cm^{-3})	V_{oc} (mV)	FF (%)	J_{sc} (mA/cm^2)	R_s (Ω cm^2)	Eff (%)	pEff (%)
1.7×10^{15}	413	64.1	19.2	2.0	5.09	5.5
5.7×10^{15}	418	61.9	17.6	3.4	4.67	5.3
1.0×10^{17}	449	62.5	6.5	7.9	2.16	2.5
8.3×10^{17}	403	54.4	4.0	19	1.04	1.3

absorber doping has a large influence on the cell efficiency varying between 1% and 5% in this series. The trends of V_{oc} as a function of N_{abs} agree very well with Suns-V_{oc} measurement results but the FF is severely affected by R_s and deviates from the pFF results. The lowest R_{sh} for all the cells is larger than 10 kΩ cm^2 and thus has only negligible impact on the cell performance. Compared with pEff, Eff is at least 0.2% (absolute) lower, and the deviation is primarily caused by R_s. This demonstrates that the combination of Suns-V_{oc} and EQE is more indicative of the material potential rather compared to light *I–V* measurements that are strongly affected by the metallization scheme in use.

B. Doping and ideality factor

It is useful to analyze the Suns-V_{oc} curves of the investigated cells more closely in terms of the ideality factors, in order to highlight an important difference in the *I–V* characteristics between the cells with different absorber doping. That is, the standard two-diode model using $n_1=1$ for quasineutral region recombination and $n_2=2$ for space charge region recombination[10,27] works well for the more heavily doped cells but fails for the lightly doped cells with absorber doping less than $\sim 1 \times 10^{16}$ cm^{-3}. Figures 6(a) and 6(b) show the measured and the standard two-diode model fitted *m*-V_{oc} curves of two cells (a) with N_{abs} of 1×10^{17} cm^{-3} and (b) with N_{abs} of 5.7×10^{15} cm^{-3}, respectively. It can be noted that the standard two-diode model fit is acceptable for the cell with higher N_{abs}, but fails for the cell with lower N_{abs}. Commonly there are three explanations for the failure of two-diode model fits: (i) a Schottky contact between the semiconductor and the measurement probes,[16] (ii) metallization-induced nonlinear shunts, or (iii) the cell contains small regions with a high recombination rate resistively isolated from the rest of the cell.[23] However, the low N_{abs} cells in this work do not fall into any one of these categories.

For the cell with low N_{abs}, we find that a significantly improved fitting can be obtained, if $n_1=1$ and $n_2=1.5$ are used, as shown in Fig. 6(b). During the fitting it could be noted that the value of n_2 is a very sensitive variable for the fitting, but adjusting n_1 (e.g., from 0.5 to 1.5) had little influence on the fit result because the n_1 diode current makes up for only a small fraction of the total recombination current in the plotted voltage range. This is in contrast to the case of the heavily doped cells, where both n_1 and n_2 diode currents play significant roles in obtaining a satisfactory two-diode model fit. The insignificant influence of n_1 in the lightly doped cells is an indicator that the space charge regions occupy a large fraction of the device volume, and the

Downloaded 26 Mar 2012 to 136.186.72.84. Redistribution subject to AIP license or copyright; see http://jap.aip.org/about/rights_and_permissions

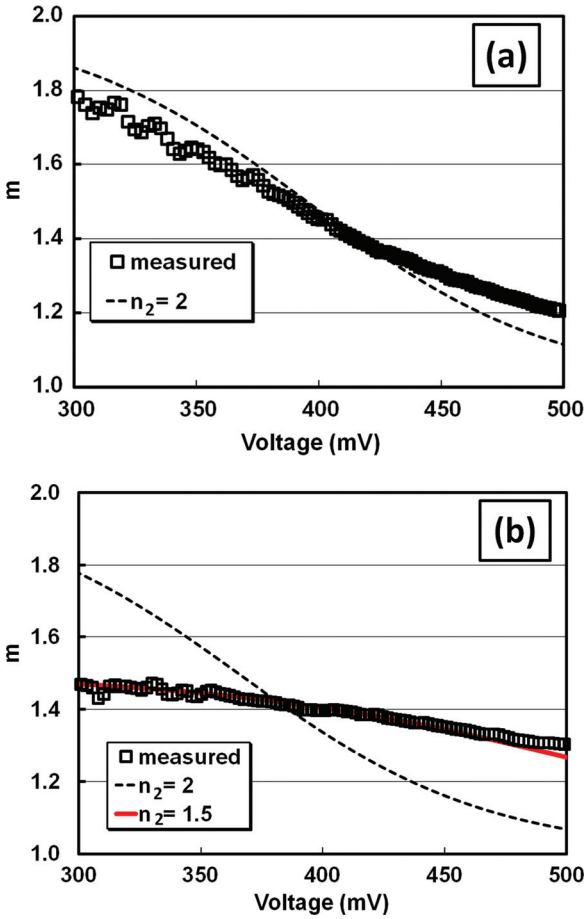

FIG. 6. (Color online) The local ideality factor m as a function of the open-circuit voltage for cells with (a) an absorber doping of 1×10^{17} cm^{-3} and (b) 5.7×10^{15} cm^{-3}. Measured data (black open squares) and standard two-diode model fits (black dashed lines) are shown for both cells. An additional fit with n_1=1 and n_2=1.5 (red solid line) are shown for the cell with 5.7×10^{15} cm^{-3} absorber doping.

Shockley–Read–Hall (SRH) recombination in the space charge region becomes the dominating factor for these cells.

It is also found that using a standard two-diode model to fit an amorphous Si (*a*-Si) or microcrystalline Si (mc-Si) *p-i-n* solar cell can prove to be difficult. Merten *et al*. therefore introduced an additional recombination term to the diode model, a current sink in parallel to the two diodes and the shunt resistance.[28] This current sink is a function of the light-generated current density and the applied voltage and depends on the quality of the intrinsic layer. This improved equivalent circuit and model was shown to successfully describe the *I–V* characteristics of these types of solar cells. Although the "emitter/lightly doped absorber/BSF" structure of the poly-Si thin-film solar cells is similar to the *p-i-n* structure, it has to be noticed that the defect densities in the absorber layer of the poly-Si cells are much lower than that in the "*i*" layer of the *a*-Si or mc-Si solar cells.

In this work, reconciling the local ideality factor data is done by changing the simplified conditions in the standard two-diode model to more general ones. The position of the trap energy level is one such consideration. Instead of assuming a single trap E_t located at the midgap, consider a trap at an energy away from the midgap $|E_t-E_i|$. In this general case the SRH recombination rate R_{SRH} can be expressed as:

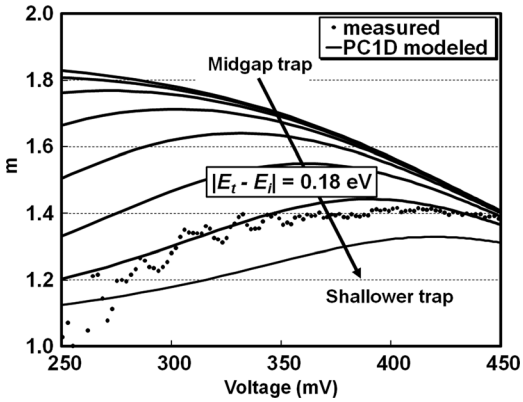

FIG. 7. PC1D modeled *m–V* curves (solid lines) for a lightly doped evaporated cell ($N_{\mathrm{abs}}=2\times10^{15}$ cm^{-3}) as a function of trap energy level $|E_t-E_i|$. The measured *m–V* curve (dotted line) is presented for comparison.

$$R_{\mathrm{SRH}}=\frac{pn-n_i^2}{\tau_p[n+n_i\exp(E_t-E_i)/kT]+\tau_n[p+n_i\exp(E_i-E_t)/kT]}, \tag{6}$$

where p and n are the concentrations of hole and electron, respectively, and n_i the intrinsic carrier concentration. Assuming the electron lifetime τ_n is equal to the hole lifetime τ_p, R_{SRH} becomes only dependent on $|E_t-E_i|$. Using this variable R_{SRH} to characterize a solar cell, the *m–V* relations of this cell can be expressed as a function of $|E_T-E_i|$. To investigate these issues PC1D was used to model the *m–V* curves as a function of $|E_T-E_i|$ and the curves were compared to the measured *m–V* curve for a lightly doped cell ($N_{\mathrm{abs}}=2\times10^{15}$ cm^{-3}). The results are shown in Fig. 7. It can be seen that the calculated *m–V* curve moves down toward unity while $|E_t-E_i|$ increases. A good match between the calculated and the measured curves is achieved when $|E_t-E_i|$=0.18 eV. A dramatic local ideality factor alteration with a small adjustment of the trap energy level is a somewhat surprising result. However, this effect is confirmed by Pallares *et al*., who made similar findings.[29] They considered the effects of different density of states of defects on the depletion region recombination for amorphous/crystalline Si heterojunctions. It was found that the ideality factor reduces from ~1.9 to ~1.25, when a single trap energy level in the amorphous side moves merely 0.1 eV away from the midgap level.

Compared with a single trap, a series of distributed traps are more realistic, but such investigations are beyond the scope of this paper. In a more detailed study with respect to the physical defects, it was proposed that shallow bands arising from the strain fields of dislocations can be the dominant recombination centers limiting the low-level injection lifetime and hence the V_{oc}.[25]

V. CONCLUSION

The effect of the absorber doping for *p*-type evaporated poly-Si thin-film solar cells on glass is studied in this work. As the absorber doping increases from $\sim2\times10^{15}$ cm^{-3} to $\sim8\times10^{17}$ cm^{-3}, the open-circuit voltage and pseudo fill factor of the *planar* cells initially increase and then decrease with the maximum values occurring at 1–2 $\times10^{17}$ cm^{-3}.

Downloaded 26 Mar 2012 to 136.186.72.84. Redistribution subject to AIP license or copyright; see http://jap.aip.org/about/rights_and_permissions

In contrast to this trend, the short-circuit current density decreases monotonically with the absorber doping. Dominated by the decreasing short-circuit current, the pseudo efficiency falls from over 6% to 1% with increasing absorber doping. Hence the absorber doping can be seen as one of the most important parameters that influence the performance of this type of solar cell.

The standard two-diode model with $n_1=1$ and $n_2=2$ is not able to satisfactorily describe the Suns-V_{oc} characteristics of the very lightly doped cells. However, a modified two-diode model with $n_2\approx1.5$ can adequately fit the experimental Suns-V_{oc} data. The low n_2 values in these cells can be modeled by a single trap energy level located at ~0.18 eV away from midgap. This finding suggests that the dominant recombination in these lightly doped cells is due to defects located some distance away from the midgap.

ACKNOWLEDGMENTS

The authors thank Johnson Wong and Thomas Söderström for valuable discussions. The Centre of Excellence for Advanced Silicon Photovoltaics and Photonics is supported under the Australian Research Council's Centres of Excellence Scheme.

[1]M. A. Green, Appl. Phys. A: Mater. Sci. Process. **A96**, 153 (2009).
[2]M. J. Keevers, T. L. Young, U. Schubert, and M. A. Green, in *Proceedings of the 22nd European Photovoltaic Solar Energy Conference, Milan, Italy,* September 2007, pp. 1783–1790.
[3]K. Yamamoto, M. Yoshimi, Y. Tawada, Y. Okamoto, A. Nakajima, and S. Igari, Appl. Phys. A: Mater. Sci. Process. **69**, 179 (1999).
[4]T. Matsuyama, N. Terada, T. Baba, T. Sawada, S. Tsuge, K. Wakisaka, and S. Tsuda, J. Non-Cryst. Solids **198**, 940 (1996).
[5]P. I. Widenborg, G. Jin, P. Gress, and S. Varlamov, *Proceedings of 24th European Photovoltaic Solar Energy Conference, Hamburg, Germany*, September 2009, pp. 2337–2340.
[6]R. Egan, M. Keevers, U. Schubert, T. Young, R. Evans, S. Partlin, M. Wolf, J. Schneider, D. Hogg, B. Eggleston, M. A. Green, F. Falk, A. Gawlik, G. Andrä, M. Werner, C. Hagendorf, P. Dogan, T. Sontheimer, and S. Gall, *Proceedings of 24th European Photovoltaic Solar Energy Conference, Hamburg, Germany*, September 2009, pp. 2279–2285.
[7]O. Kunz, Z. Ouyang, S. Varlamov, and A. G. Aberle, Prog. Photovoltaics **17**, 567 (2009).
[8]Z. Ouyang, S. Pillai, F. Beck, O. Kunz, S. Varlamov, K. R. Catchpole, P. Campbell, and M. A. Green, Appl. Phys. Lett. **97**, 261109 (2010).
[9]J. Wong, J. L. Huang, O. Kunz, Z. Ouyang, S. He, P. I. Widenborg, A. G. Aberle, M. Keevers, and M. A. Green, J. Appl. Phys. **105**, 103705 (2009).
[10]M. A. Green, *Solar Cells: Operating Principles, Technology and System Applications* (The University of New South Wales, Sydney, 1998).
[11]S. Narayanan, S. R. Wenham, and M. A. Green, Appl. Phys. Lett. **48**, 873 (1986).
[12]A. Straub, "Polycrystalline silicon thin-film solar cells on glass by ion-assisted deposition," Ph.D. thesis, The University of New South Wales Sydney, 2005.
[13]D. A. Clugston and P. A. Basore, Record of 26th IEEE Photovoltaic Specialists Conference, Anaheim, September 1997, pp. 207–210.
[14]O. Kunz, Z. Ouyang, J. Wong, and A. G. Aberle, *Proceedings of Conference on Optoelectronic and Microelectronic Materials and Devices, Sydney, Australia, July* 2008, pp. 289–292.
[15]A. Straub, R. Gebs, H. Habenicht, S. Trunk, R. A. Bardos, A. B. Sproul, and A. G. Aberle, J. Appl. Phys. **97**, 083703 (2005).
[16]R. A. Sinton and A. Cuevas, *Proceedings of 16th European Photovoltaic Solar Energy Conference, Glasgow, UK*, May 2000, pp. 1152–1155.
[17]O. Kunz, D. Inns, A. B. Sproul, and A. G. Aberle, *Proceedings of the 21st European Photovoltaic Solar Energy Conference, Dresden, Germany, September* 2006, pp. 374–377.
[18]S. Bowden, V. Yelundur, and A. Rohatgi, Record of the 29th IEEE Photovoltaic Specialists Conference, New Orleans, May 2002, pp. 371–374.
[19]A. G. Aberle, S. R. Wenham, and M. A. Green, Record of the 23rd IEEE Photovoltaic Specialists Conference, New York, May 1993, pp. 133–139.
[20]M. Wolf and H. Rauschenbach, Adv. Energy Convers. **3**, 455 (1963).
[21]A. Luque and S. Hegedus, *Handbook of Photovoltaic Science and Engineering* (Wiley, Chichester, 2003).
[22]O. Kunz, R. Brüggemann, A. Straub, A. B. Sproul, and A. G. Aberle, *Proceedings of the 20th European Photovoltaic Solar Energy Conference, Barcelona, Spain,* June 2005, pp. 226–229.
[23]K. McIntosh, "Lumps, humps, and bumps: Three detrimental effects in the current-voltage curve of silicon solar cells," Ph.D. thesis, The University of New South Wales, Sydney, 2001.
[24]R. Brendel, *Thin-Film Crystalline Silicon Solar Cells: Physics and Technology* (Wiley, Weinheim, 2003).
[25]J. Wong, J. L. Huang, B. Eggleston, M. A. Green, O. Kunz, R. Evans, M. Keevers, and R. J. Egan, J. Appl. Phys. **107**, 123705 (2010).
[26]M. L. Terry, A. Straub, D. Inns, D. Song, and A. G. Aberle, Appl. Phys. Lett. **86**, 172108 (2005).
[27]S. M. Sze and K. K. Ng, *Physics of Semiconductor Devices*, 3rd ed. (Wiley, Hoboken, 2007).
[28]J. Merten, J. M. Asensi, C. Voz, A. V. Shah, R. Platz, and J. Andreu, IEEE Trans. Electron Devices **45**, 423 (1998).
[29]J. Pallares, L. F. Maarsal, X. Correig, J. Calderer, and R. Alcubilla, Solid-State Electron. **41**, 17 (1997).

Downloaded 26 Mar 2012 to 136.186.72.84. Redistribution subject to AIP license or copyright; see http://jap.aip.org/about/rights_and_permissions